J. Fluid Mech. (1991), *vol.* 230, *pp.* 479–504
Printed in Great Britain

The rate of collisions due to Brownian or gravitational motion of small drops

By XIAOGUANG ZHANG AND ROBERT H. DAVIS†
Department of Chemical Engineering, University of Colorado, Boulder, CO 80309-0424, USA

(Received 30 November 1990 and in revised form 5 March 1991)

A dilute dispersion containing drops of one fluid dispersed in a second, immiscible fluid is considered. The drops are sufficiently small that inertia is negligible and that they remain spherical. Two drops of different size are in relative motion due to either Brownian diffusion or gravitational sedimentation. When the drops become close, they interact with each other owing to hydrodynamic disturbances and van der Waals attractions, and, under favourable conditions, they will collide with each other and coalesce. The rate at which two drops collide is predicted by solving the diffusion equation for Brownian coalescence, and by using a trajectory analysis to follow the relative motion of pairs of drops for gravity-induced coalescence.

The emphasis of our analysis is on the effects of drop interactions on their collision rate, and these are described by the collision efficiency. Since the hydrodynamic resistance to the drop relative motion reduces with a decreasing ratio of the viscosities of the drop fluid and the surrounding fluid, the collision efficiency increases with decreasing viscosity ratio. A qualitative difference in the collision behaviour of viscous drops from that of rigid spheres is demonstrated; finite collision rates for drops are predicted even in the absence of attractive forces, provided that drop deformation is negligible, whereas rigid particles with smooth surfaces will not come into contact in a fluid continuum unless an attractive force is present which is able to overcome the lubrication forces resisting the relative motion. Hydrodynamic interactions between two spherical drops are accounted for exactly by determining the two-sphere relative mobility functions from previous solutions for two drops moving along and normal to their line of centres. These solutions are based on the method of reflections for widely separated drops, lubrication theory for drops in near-contact, and bispherical coordinates for general separations. The hydrodynamic interactions have a greater effect on reducing the rate of gravity collisions than the rate of Brownian collisions.

1. Introduction

Drop collisions and coalescence play important roles in a variety of natural and industrial phenomena, such as raindrop growth, liquid–liquid extraction, and the processing of bimetallic composite materials exhibiting a liquid-phase miscibility gap. In this paper, we predict collision rates for small drops in a dilute, statistically homogeneous dispersion. The drops are of different sizes and are in relative motion due to their different settling speeds induced by gravity or due to their random Brownian motion. It is assumed that the drops are sufficiently small (typically having diameters of approximately 100 μm, or less) that they remain spherical due to their interfacial tension and that inertia is small relative to viscous forces. When

† To whom correspondence should be addressed.

two drops are within several radii of each other, hydrodynamic interactions resist their relative motion and cause them to flow around each other. If the drops become sufficiently close to one another, they exert an attractive van der Waals force on each other which pulls them together. When the drops come into physical contact, they will coalesce into a single, larger drop due to the tendency of interfacial tension to minimize the surface area and surface energy of the contacted drops (Melik 1984). As a result of drop collisions and coalescence, the drop sizes in a dispersion will increase over time from the initial distribution. This change in the drop number density versus size distribution represents a *macrophysical* problem that is typically solved using population dynamics equations (Rogers & Davis 1990). These equations include collision kernels which contain the collision rate between two drop size categories. The focus of the present paper is to provide this required information by solving the *microphysical* problem of two interacting drops in order to predict the collision rate, given the instantaneous number densities of the two size categories. The drops are allowed to have an arbitrary size ratio and an arbitrary viscosity ratio relative to the surrounding fluid. It is assumed that changes to the drop sizes (such as by dissolution or breakup) are negligible over the timescale of a collision.

It is well known that lubrication forces prevent rigid particles with smooth surfaces from coming into physical contact in the absence of an attractive force which increases without bound as the separation between the surfaces decreases. In contrast, when drops approach each other in near contact, the mobility of their interfaces allows the fluid between them to be squeezed outward with much less resistance than for the rigid particle case. As discussed by Davis, Schonberg & Rallison (1989), this allows for non-zero collision rates of non-deforming drops, even in the absence of attractive forces.

Relative motion, collisions, and coagulation of rigid spheres induced by gravity sedimentation or by Brownian diffusion have been investigated extensively. Smoluchowski (1917) made the first attempt to estimate the rate of coagulation in a dilute dispersion. In his classical model, the rigid spheres were assumed to move independently, without any hydrodynamic interactions or interparticle forces other than a sticking force upon contact. Accounting for the simultaneous effects of hydrodynamic interactions and interparticle attractive and repulsive forces, Spielman (1970) developed a theoretical model to predict the rate of coagulation for monodispersed rigid spheres subject to Brownian diffusion. Valioulis & List (1984) and Kim & Zukoski (1990) performed similar calculations for heterodispersed rigid spheres. These authors solved the steady-state diffusion equation describing the relative Brownian motion between two coagulating particles. For gravity-induced coagulation of rigid spheres with hydrodynamic and interparticle forces, theoretical models have been developed by Davis (1984) and by Melik & Fogler (1984) to predict the rate of coagulation using trajectory analyses, and by Wen & Batchelor (1984) using an asymptotic method for solving the convective-diffusion equation. All of these studies show that the hydrodynamic resistance to relative motion causes the collision rates to approach zero as the attractive forces become weak.

There are fewer studies of the coalescence of fluid drops, presumably because of the more complex interactions which involve fluid flow both inside and outside of the drops and which include the possibility that the drops will deform as they collide. A notable exception is that Zinchenko (1982) has calculated the rate of gravity-induced coalescence of spherical drops of different sizes numerically using a trajectory analysis for pairs of drops, without considering the effects of interparticle forces. His results confirm that, in contrast to rigid spheres, drop collision is possible at finite

rates under the action of a finite external force only. He also showed how the rate of drop collisions decreases with an increasing ratio of the drop fluid viscosity and the surrounding fluid viscosity.

Under conditions of low Reynolds numbers, the relative motion of two spherical drops may be decomposed into motions along and normal to their line of centres. Hetsroni & Haber (1978) used the method of reflections to describe the hydrodynamic interaction for widely separated drops in both configurations. More accurate image techniques, which are valid unless the separation distance is small relative to the radius of the smaller drop, have been developed by Fuentes, Kim & Jeffrey (1988, 1989). Exact solutions – based on bispherical coordinate methods – have been developed by Haber, Hestroni & Solan (1973) and Rushton & Davies (1973) for axisymmetric motion along the line of centres, and by Zinchenko (1980) for asymmetric motion normal to the line of centres. Each of these solution methods yields an infinite series for the hydrodynamic force between the drops, which diverges when the distance between the drops tends to zero. Because coalescence phenomena depend critically on the near-contact interaction, these earlier solutions may be matched with the recent lubrication theory results of Davis *et al.* (1989), in which the nature of the hydrodynamic force resisting the near-contact relative motion of two spherical drops in the direction along their line of centres has been analysed in detail.

The present work employs the above solutions for the hydrodynamic interactions of two spherical drops and calculates collision rates by extending the previous work by several authors for rigid particles and by Zinchenko (1982) for spherical drops. In §2, the effects of drop interactions on their relative motion are discussed. Previous solutions for the hydrodynamic interactions are collected and presented in useful forms as two-sphere relative mobility functions for drops. In §3, theoretical models are developed for Brownian coalescence and gravity-induced coalescence. An expression for the collision rate of Brownian drops is developed by analytically solving the diffusion equation, and a trajectory analysis is used to determine the collision rate of sedimenting drops. We do not consider the combined effects of gravity sedimentation and Brownian motion here, and so the analysis applies only in the limits of large Péclet numbers (gravity-dominated collisions) and small Péclet numbers (Brownian-dominated collisions). In §4, the results of the analytical and numerical computations for Brownian and gravity-induced collisions are presented and discussed. Most of the results are presented in dimensionless form, with an exception made for illustrative purposes for typical hydrosol dispersions. Concluding remarks are given in §5.

2. Interactions between spherical drops

2.1. *Expression for the relative velocity of two drops*

We consider a dilute dispersion containing spherical drops of viscosity μ' and density ρ' dispersed in an immiscible fluid of viscosity μ and density ρ. Both fluids are Newtonian and isothermal, and it is assumed that there are no surfactants on the drop surfaces. For dilute dispersions, the probability of a third drop influencing the relative motion of two interacting drops is small, and so the analysis is restricted to binary interactions of drops with radii a_1 and a_2, as shown in figure 1. For creeping flow, the external driving forces on each drop balance the hydrodynamic forces, and the velocity $\boldsymbol{V}_{12}$ of drop 1 relative to drop 2 is linearly related to the sum of the external forces and depends only on the relative position of the two drops. An

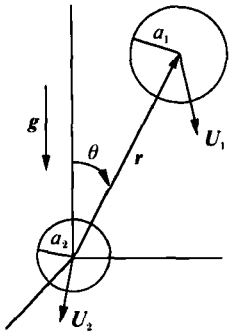

FIGURE 1. Schematic of the coordinate system used for the relative motion of two different-sized drops.

expression for this relative velocity has been presented by Bachelor (1982) for rigid spheres, the essential details of which are modified here for spherical drops:

$$\boldsymbol{V}_{12}(\boldsymbol{r}) = \boldsymbol{V}_{12}^{(0)}\cdot\left[\frac{\boldsymbol{rr}}{r^2}L(s)+\left(\boldsymbol{I}-\frac{\boldsymbol{rr}}{r^2}\right)M(s)\right]-\frac{D_{12}^{(0)}}{kT}\left[\frac{\boldsymbol{rr}}{r^2}G(s)+\left(\boldsymbol{I}-\frac{\boldsymbol{rr}}{r^2}\right)H(s)\right]\cdot\nabla(\boldsymbol{\Phi}_{12})$$
$$-D_{12}^{(0)}\left[\frac{\boldsymbol{rr}}{r^2}G(s)+\left(\boldsymbol{I}-\frac{\boldsymbol{rr}}{r^2}\right)H(s)\right]\cdot\nabla(\ln p_{12}(\boldsymbol{r})), \quad (2.1)$$

where $\boldsymbol{r}$ is the vector from the centre of drop 2 to the centre of drop 1 and $\boldsymbol{I}$ is the unit second-order tensor.

The relative velocity due to gravity for two widely separated drops is given by the Hadamard–Rybczynski formula (Lamb 1945):

$$\boldsymbol{V}_{12}^{(0)} \equiv \boldsymbol{U}_1^{(0)} - \boldsymbol{U}_2^{(0)} = \frac{2(\hat{\mu}+1)(\rho'-\rho)a_1^2(1-\lambda^2)\boldsymbol{g}}{3(3\hat{\mu}+2)\mu}, \quad (2.2)$$

where $\hat{\mu} = \mu'/\mu$ is the viscosity ratio, $\lambda = a_2/a_1$ is the radius ratio, $\boldsymbol{g}$ is the gravitational acceleration vector, and $\boldsymbol{U}_i^{(0)}$ is the settling velocity of an isolated drop. Similarly, the relative diffusivity due to Brownian motion for two widely separated drops is

$$D_{12}^{(0)} = \frac{kT(\hat{\mu}+1)(1+\lambda^{-1})}{2\pi\mu(3\hat{\mu}+2)a_1}, \quad (2.3)$$

where $k = 1.381\times10^{-16}$ erg/K is Boltzmann's constant and T is the absolute temperature.

The pair-distribution function, $p_{12}(\boldsymbol{r})$, represents the probability that drop 1 is at position $\boldsymbol{r}$ relative to drop 2, normalized such that $p_{12}\to 1$ as $r\to\infty$. The interparticle force is described by the potential function $\boldsymbol{\Phi}_{12}(\boldsymbol{r})$, which is discussed in more detail in the following section.

The relative mobility functions for motion along the line of centres (L and G) and motion normal to the line of centres (M and H) describe the effects of hydrodynamic interactions between the two drops. These functions depend on the size ratio of two drops, λ, the viscosity ratio of the drop fluid and the surrounding fluid, $\hat{\mu}$, and the dimensionless distance between the drops, $s = 2r/(a_1+a_2)$, and they are unchanged when λ is replaced with λ^{-1}. Analytical expressions and numerical values of these functions for arbitrary values of λ, $\hat{\mu}$, and s are available in the literature and are discussed in §2.3 of this paper.

The three terms on the right-hand side of (2.1) represent the contributions of gravity, interparticle forces, and Brownian diffusion to the drop relative motion,

respectively. Their relative importance may be measured by a dimensionless interparticle force parameter, Q_{12}, and the Péclet number, Pe, as defined by Davis (1984):

$$Q_{12} \equiv \frac{\frac{1}{2}(a_1+a_2)\,V_{12}^{(0)}}{AD_{12}^{(0)}/kT}; \quad Pe \equiv \frac{\frac{1}{2}(a_1+a_2)\,V_{12}^{(0)}}{D_{12}^{(0)}},$$

where $V_{12}^{(0)} = |\boldsymbol{V}_{12}^{(0)}|$ is the magnitude of the relative velocity of two widely separated drops, and A is the composite Hamaker constant, which is chosen as a measure of the strength of the interparticle forces (see §2.2). Note that the Péclet number is proportional to the fourth power of the drop radius. For typical hydrosols and aerosols, $Pe \gg 1$ when the radii of the drops are larger than about 2 μm, and so gravity sedimentation dominates over Brownian diffusion for such drops. Also, since $Q_{12} = Pe\,kT/A$, and kT/A is typically of order unity for hydrosols and of order 10^{-1} for aerosols (Davis 1984), the restriction that Pe is large will also require that Q_{12} be large, and the contribution of the interparticle forces to the drop relative motion is then small, except when the drops are very close to one another. On the other hand, $Pe \ll 1$ for submicron drops, and so Brownian diffusion and interparticle forces dominate over gravity sedimentation for such very small drops.

Carrying out the vector and tensor operations indicated by (2.1), and non-dimensionalizing the relative velocity with $V_{12}^{(0)}$, gives

$$\boldsymbol{u}_{12} = -L(s)\cos\theta\,\boldsymbol{e}_r + M(s)\sin\theta\,\boldsymbol{e}_\theta - \frac{1}{Q_{12}}G(s)\frac{\mathrm{d}\phi_{12}}{\mathrm{d}s}\boldsymbol{e}_r - \frac{1}{Pe}\left[G(s)\frac{\partial}{\partial s}(\ln p_{12})\,\boldsymbol{e}_r + \frac{H(s)}{s}\frac{\partial}{\partial\theta}(\ln p_{12})\,\boldsymbol{e}_\theta\right], \quad (2.4)$$

where $\boldsymbol{u}_{12}$ is the dimensionless relative velocity, $\boldsymbol{e}_r$ and $\boldsymbol{e}_\theta$ are unit vectors in the radial and tangential directions in a spherical polar coordinate system (see figure 1), respectively, and $\phi_{12} = \Phi_{12}/A$ is the dimensionless interparticle potential scaled with the Hamaker constant. It is assumed in (2.4) that the interparticle force acts only along the line of centres.

2.2. *The interparticle force potential*

The most commonly used interparticle potential model is described by the DLVO theory attributed to Derjaguin & Landau (1941) and Verwey & Overbeek (1948), which assumes that the total interparticle potential is obtained by summing the individual attractive and repulsive contributions. The attractive van der Waals force is responsible for pulling nearby drops into contact and holding contacted drops together during coalescence, whereas the electrostatic repulsion gives rise to a repulsive energy barrier that may prevent the drops from becoming sufficiently close to be pulled into contact. Repulsive forces between drops are generally associated with the presence of surfactants on the drop interfaces. Since surfactants modify the mobility of the interfaces (by a variety of mechanisms to make them more rigid), their presence would violate an underlying restriction of this paper, that the external flow is able to drive an internal flow within the drops that is resisted only by their viscosity and not by tangential interfacial stresses. Thus, we consider here only clean interfaces for which the interparticle force is dominated by van der Waals attraction. In the colloid literature, the absence of repulsive forces is referred to as 'rapid' coagulation or coalescence. Limited results which include repulsive forces between drops are given by Zhang (1992).

The van der Waals force between isolated drops was first calculated by Hamaker

(1937) using a pairwise additivity theory. For unequal spheres, the force potential as a function of the drop separation is then

$$\Phi_{12} = -\frac{A}{6}\left\{\frac{8\lambda}{(s^2-4)(1+\lambda)^2}+\frac{8\lambda}{s^2(\lambda+1)^2-4(1-\lambda)^2}+\ln\left[\frac{(s^2-4)(1+\lambda)^2}{s^2(1+\lambda)^2-4(1-\lambda)}\right]\right\}. \quad (2.5)$$

The Hamaker calculation neglects electromagnetic retardation and hence is valid only for separations between drops less than the London wavelength, λ_L, which is typically of order 0.1 μm. Schenkel & Kitchner (1960) made a detailed analysis of this retardation effect and derived empirical expressions by following best-fit approximations to their numerical integrations for $\xi \equiv s-2 \ll 1$. Their results are applicable only for equal-sized spheres; however, Ho & Higuchi (1968) used similar procedures to obtain the interactions between unequal-sized spheres:

$$\Phi_{12} \approx \frac{A}{3(s-2)}\frac{\lambda}{(1+\lambda)^2}Z(p_0), \quad (2.6)$$

where

$$\left.\begin{aligned} Z(p_0) &= \frac{1}{1+1.7692p_0} \quad \text{for } p_0 \leqslant 1.0,\\ Z(p_0) &= \frac{2.45}{5p_0}-\frac{2.17}{15p_0^2}+\frac{0.59}{25p_0^3} \quad \text{for } p_0 > 1.0,\end{aligned}\right\} \quad (2.7)$$

with $p_0 = 2\pi\xi/\nu$ and $\nu = 2\lambda_L/(a_1+a_2)$. The dimensionless parameter ν is used to determine the degree of retardation. As ν increases (i.e. the size of the drops decreases), the retardation is of increasing importance and reduces the attractive force.

2.3. *Mobility functions for the relative motion of two drops*

Considerable progress has been made in recent years on the hydrodynamic interactions between two spherical drops in axisymmetric motion along their line of centres and asymmetric motion normal to their line of centres. A far-field asymptotic solution for the resistance functions (which specify the hydrodynamic forces given the drop velocities) in power series $1/s$ up to order $1/s^6$ has been derived using the method of reflections (Hetsroni & Haber 1978). From these, analytical expressions for the relative mobility functions L, G, M, and H can be deduced (contact the authors or see Zhang 1992 for details):

$$L(s) = 1-\frac{2+3\hat{\mu}}{1+\hat{\mu}}\frac{\lambda^3-1}{(1+\lambda)(\lambda^2-1)}\frac{1}{s}+4\frac{\hat{\mu}}{1+\hat{\mu}}\frac{(\lambda^3-1)(\lambda^2+1)}{(1+\lambda)^3(\lambda^2-1)}\frac{1}{s^3}+O\left(\frac{1}{s^6}\right), \quad (2.8)$$

$$G(s) = 1-2\frac{2+3\hat{\mu}}{1+\hat{\mu}}\frac{\lambda}{(1+\lambda)^2}\frac{1}{s}+8\frac{\hat{\mu}}{1+\hat{\mu}}\frac{\lambda(\lambda^2+1)}{(1+\lambda)^4}\frac{1}{s^3} -4\frac{(2+5\hat{\mu})(2+3\hat{\mu})}{(1+\hat{\mu})^2}\frac{\lambda(\lambda^3+1)}{(1+\lambda)^5}\frac{1}{s^4}+O\left(\frac{1}{s^6}\right), \quad (2.9)$$

$$M(s) = 1-\frac{3\hat{\mu}+2}{2(\hat{\mu}+1)}\frac{\lambda^3-1}{(1+\lambda)(\lambda^2-1)}\frac{1}{s}-2\frac{\hat{\mu}}{1+\hat{\mu}}\frac{(\lambda^3-1)(\lambda^2+1)}{(1+\lambda)^3(\lambda^2-1)}\frac{1}{s^3}+O\left(\frac{1}{s^6}\right), \quad (2.10)$$

$$H(s) = 1-\frac{3\hat{\mu}+2}{\hat{\mu}+1}\frac{\lambda}{(1+\lambda)^2}\frac{1}{s}-2\frac{\hat{\mu}}{1+\hat{\mu}}\frac{\lambda^3-\lambda}{(1+\lambda)^2}\frac{1}{s^3}+O\left(\frac{1}{s^6}\right). \quad (2.11)$$

For two arbitrarily separated drops, more comprehensive solutions – based on the method of bispherical coordinates – have been developed by Haber *et al.* (1973) and

by Rushton & Davies (1973) for axisymmetric motion, and by Zinchenko (1980) for asymmetric motion. These solutions for the resistance functions allow for numerical calculation of the relative mobility functions for complete ranges of the parameters λ and $\hat{\mu}$ using infinite series which may be truncated when the desired convergence is reached. Unfortunately, these exact solutions require an increasingly large number of terms for convergence, and show that the hydrodynamic force opposing a prescribed relative motion increases without bound, as the distance between the drops becomes very small. The image solutions of Fuentes *et al.* (1988, 1989) are easier to use than the bispherical coordinate solutions – especially for transverse motion. Unfortunately, they are not sufficiently accurate at small separations for the purposes of our study of drop collisions.

In order to overcome the convergence difficulties, and to elucidate the exact nature of the singularity as the drops become very close to one another, lubrication theory is used for analysing the near-contact interactions of two drops in axisymmetric motion. In the development of Davis *et al.* (1989), the dimensionless lubrication force between two spherical drops in near contact is shown to depend on a single dimensionless parameter, $m \equiv \hat{\mu}^{-1}(a/h_0)^{\frac{1}{2}}$, where $a \equiv a_1 a_2/(a_1+a_2)$ is the reduced radius of the two drops and $h_0 = r-(a_1+a_2)$ is the closest separation between two drop surfaces. This parameter describes the mobility of the interfaces: when $m \ll 1$, the drops behave as rigid spheres, whereas when $m \gg 1$, the drops have fully mobile interfaces and offer relatively little resistance to the drop relative motion. Note that the interface mobility, m, is not a property of the interfaces themselves but instead represents the viscous resistance of the fluid inside the drops to the flow exerted on their interfaces by the external fluid as it is squeezed out of the gap between the drops. Using this interface mobility, the lubrication forces acting on drops in the direction along their line of centres can be simply expressed as

$$-F_{1,1} = F_{1,2} = 6\pi\mu a^2 \frac{V_{12}}{h_0} f(m), \tag{2.12}$$

where V_{12} is the component of $\boldsymbol{V}_{12}$ in the direction along the line of centres, and $f(m)$ is a dimensionless function which is approximated by Davis *et al.* (1989) using the following Padé-type expression:

$$f(m) = \frac{1+0.402m}{1+1.711m+0.461m^2}. \tag{2.13}$$

Note that the lubrication force for drops with mobile interfaces ($m \gg 1$) is inversely proportional to $(h_0/a)^{\frac{1}{2}}$, indicating that spherical drops can come into contact in a finite time under the action of a fine force, in contrast to that for immobile interfaces ($m \ll 1$) for which the lubrication force is inversely proportional to h_0/a. This lubrication force dominates the hydrodynamic resistance unless the drop viscosity is very small ($\hat{\mu} < O(h_0/a)^{\frac{1}{2}}$), in which case the fluid slips out of the gap with little resistance.

The primary task remaining for the drop relative motion along the line of centres is to determine the functions L and G for near-contact drops using the results described above. To do this, we consider two unequal drops which are nearly touching and which move together as a pair with velocity U_p due to gravity acting along their line of centres. Superimposed on this is a small relative velocity of the larger drop approaching the smaller one. A force balance on each drop yields

$$F_{g,i}+F_{d,i}+F_{1,i} = 0, \tag{2.14}$$

λ	$\hat{\mu}$	0	0.1	0.5	1.0	2.0	5.0	10	20	100	10^3
0.15	L_1	—	0.660	0.657	0.644	0.597	0.507	0.438	0.379	0.309	0.280
	C_0	0.642	0.668	0.729	0.759	0.789	1.342	—	—	—	—
	M_0	0.555	0.519	0.424	0.357	0.287	0.209	0.167	0.136	0.096	0.079
	M_1	0.976	1.136	1.446	1.558	1.611	2.570	3.435	7.370	32.771	52.835
0.25	L_1	—	0.696	0.706	0.691	0.658	0.585	0.527	0.484	0.421	0.398
	C_0	0.644	0.668	0.718	0.731	0.722	1.218	—	—	—	—
	M_0	0.578	0.545	0.460	0.401	0.338	0.268	0.228	0.197	0.153	0.129
	M_1	0.441	0.500	0.523	0.563	0.813	1.385	2.350	5.073	24.166	45.688
0.5	L_1	—	0.786	0.817	0.823	0.810	0.766	0.730	0.698	0.656	0.639
	C_0	0.651	0.669	0.696	0.669	0.567	0.872	—	—	—	—
	M_0	0.606	0.579	0.508	0.458	0.407	0.349	0.316	0.290	0.251	0.228
	M_1	0.222	0.261	0.274	0.330	0.416	0.977	1.417	3.493	16.833	38.596
0.9	L_1	—	0.835	0.880	0.898	0.899	0.874	0.848	0.824	0.791	0.777
	C_0	0.656	0.666	0.658	0.579	0.352	0.340	—	—	—	—
	M_0	0.619	0.594	0.528	0.482	0.436	0.385	0.356	0.334	0.301	0.281
	M_1	0.159	0.178	0.233	0.282	0.350	0.559	0.996	2.085	9.665	32.017

TABLE 1. Values of the parameters L_1, C_0, M_0, and M_1 that appear in the near-field expressions for the relative mobility functions.

where $F_{g,i}$ is the gravity force acting on the drop i, which can be described by the Hadamard–Rybczynski result:

$$F_{g,i} = 6\pi\mu a_i U_i^{(0)} \frac{3\hat{\mu}+2}{3\hat{\mu}+3}. \tag{2.15}$$

$F_{d,i}$ is the drag force exerted on the drop i by the surrounding fluid, and is defined as the total hydrodynamic force minus the lubrication force. According to the analysis of Reed & Morrison (1974) for two touching drops, it can be expressed as:

$$F_{d,i} = -6\pi\mu a_i U_p \frac{3\hat{\mu}+2}{3\hat{\mu}+3}\beta_i, \tag{2.16}$$

where β_i is a correction factor to the Hadamard–Rybczynski formula for drop i to account for the presence of the second drop.

Equations (2.14)–(2.16) for $i = 1$ and $i = 2$ may be solved for the pair velocity U_p and the lubrication force, $F_{l,1} = -F_{l,2}$. Using the latter in (2.1) and (2.12) yields the near-field asymptotic solution for L, after some algebra:

$$L(\xi) = \frac{3\hat{\mu}+2}{3\hat{\mu}+3}\frac{(1+\lambda)^3}{4\lambda^2(\lambda^2-1)}\left[\lambda^3-1-(\lambda\beta_2-\beta_1)\frac{1+\lambda^3}{\beta_1+\lambda\beta_2}\right]\frac{\xi}{f(m)}. \tag{2.17}$$

The factors β_1 and β_2, which depend on λ and $\hat{\mu}$, were calculated by the method of Reed & Morrison (1974). The results for the entire coefficient on the right-hand side of (2.17),

$$L_1 \equiv \frac{3\hat{\mu}+2}{3\hat{\mu}+3}\frac{(1+\lambda)^3}{4\lambda^2(\lambda^2-1)}\left[\lambda^3-1-(\lambda\beta_2-\beta_1)\frac{1+\lambda^3}{\beta_1+\lambda\beta_2}\right],$$

are given in table 1.

The derivation of the asymptotic solution for G for two near-contact drops is relatively simple because this function describes the effect of equal but opposite external forces exerted on the two drops (such as the interparticle force, $\nabla(\Phi_{12})$, or the thermodynamic force, $kT\nabla(\ln p_{12}(r))$. When the drops are close to one another

($\xi \to 0$), the lubrication force dominates the hydrodynamic force and directly balances the external force on each of the drops. Using (2.12) in (2.1) then yields the near-field solution for G:

$$G(\xi) = \frac{2+3\hat{\mu}}{3+3\hat{\mu}} \frac{(1+\lambda)^2}{2\lambda} \frac{\xi}{f(m)}. \tag{2.18}$$

As discussed by Davis *et al.* (1989), the lubrication force in the near-contact region does not dominate the remaining hydrodynamic force around the drops when the viscosity ratio is very small. Instead, the functions L and G may be determined by examining the bispherical-coordinate solution in the limit as the drops become close. From the arguments by Zinchenko (1978, 1982) for the asymptotic, near-field expansions of the resistance functions, it may be shown that the limit $\xi \ll 1$ with $m \gg 1$ yields

$$L = \frac{(\lambda^2\beta_1 - \beta_2)\dfrac{3\hat{\mu}+2}{3\hat{\mu}+3}}{(\lambda^2-1)\left[A\left(\beta_2 + \dfrac{1}{\lambda}\beta_1\right) - \dfrac{1}{\lambda}\beta_1^2 \dfrac{3\hat{\mu}+2}{3\hat{\mu}+3}\right]}, \tag{2.19}$$

and

$$G = \frac{(\beta_1 + \lambda\beta_2)\dfrac{3\hat{\mu}+2}{3\hat{\mu}+3}}{(1+\lambda)\left[A\left(\beta_2 + \dfrac{1}{\lambda}\beta_2\right) - \dfrac{1}{\lambda}\beta_1^2 \dfrac{3\hat{\mu}+2}{3\hat{\mu}+3}\right]}, \tag{2.20}$$

where A represents the asymptotic solution for the resistance function and is expressed by Zinchenko (1978, 1982) as

$$A = \frac{\pi^2\sqrt{2\,\hat{\mu}}}{16(1+1/\lambda)^{\frac{3}{2}}}\left(\frac{2}{\xi(1+\lambda)}\right)^{\frac{1}{2}} + \frac{\lambda}{3(1+\lambda)}\left(1 - \frac{\hat{\mu}^2}{3}\right)\ln\left(\xi\frac{(1+\lambda)}{2}\right)^{-1} + C_0.$$

C_0 is a parameter of order unity which depends on λ and $\hat{\mu}$; typical values are given in table 1. Although (2.19) and (2.20) are restricted to drops which have sufficiently mobile interfaces, that is $m \gg 1$, it is particularly useful for drops of small viscosity for which $\hat{\mu}$ is comparable to or smaller than $(h_0/a)^{\frac{1}{2}}$ and for which (2.17) and (2.18) are then invalid.

No asymptotic solution for hydrodynamic interactions between two drops in near-contact relative motion normal to their line of centres is available. However, from the numerical calculations of Zinchenko (1980) and Fuentes *et al.* (1989), it is expected that the mobility function, M, for two viscous drops with mobile interfaces has no singularity and that the lubrication force does not make a substantial contribution to the hydrodynamic interactions between two drops moving in near-contact normal to their line of centres. Thus, a simple expansion for $\xi \ll 1$ gives

$$M(\xi) = M_0 + M_1\xi + O(\xi^2), \tag{2.21}$$

where M_0 and M_1 are parameters, given in table 1, depending on $\hat{\mu}$ and λ which we have determined approximately by fitting the exact solution for M using the method of least squares. These results for drops are in contrast to those for rigid spheres which show a logarithmic singularity for near-contact transverse motion. Similar results for the relative mobility function H may be obtained, but these are not discussed here because they are not needed for the calculations described in this paper.

Typical results of the asymptotic solutions for L, G, and M as functions of the dimensionless distance between two drop surfaces, $\xi \equiv s-2$, for widely separated

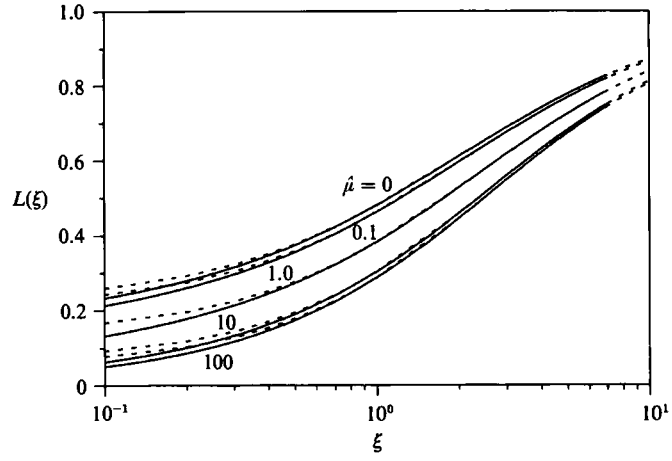

FIGURE 2. The relative mobility function L for axisymmetric motion of two spherical drops as a function of the dimensionless distance between drop surfaces for $\lambda = 0.5$, with different $\hat{\mu}$. The solid lines are from the exact solution; the dashed lines are from the far-field solution given by (2.8).

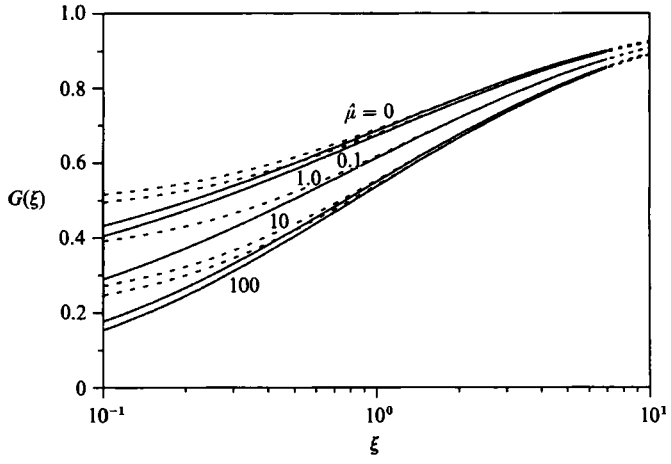

FIGURE 3. The relative mobility function G for axisymmetric motion of two spherical drops as a function of the dimensionless distance between drop surfaces for $\lambda = 0.5$, with different $\hat{\mu}$. The solid lines are from the exact solution; the dashed lines are from the far-field solution given by (2.9).

drops ((2.8), (2.9), and (2.10)) and for near-contact drops ((2.17), (2.18), and (2.21)) are plotted as dashed lines in figures 2–4 and figures 5–7, respectively, for $\lambda = 0.5$, and a variety of viscosity ratios. For comparison, the corresponding exact solutions using the methods of bispherical coordinates are also shown in these figures as solid lines. We calculated the latter numerically in a high-precision VAX computer system, using the solution of Haber *et al.* (1973) for motion along the line of centres and the solution of Zinchenko (1980) for motion normal to the line of centres. Details of these calculations may be obtained from the authors or from Zhang (1992).

As expected, the asymptotic solutions are in very good agreement with the exact ones within certain ranges of the drop separation. The far-field expansions are accurate to within a few percent for separations as small as one drop radius for motion along the line of centres (L and G), and for even smaller separations for motion normal to the line of centres (M). In fact, the far-field expansions for M may be used for $\hat{\mu} \leqslant 1$ for all separations, with an error of less than 1%. The near-field

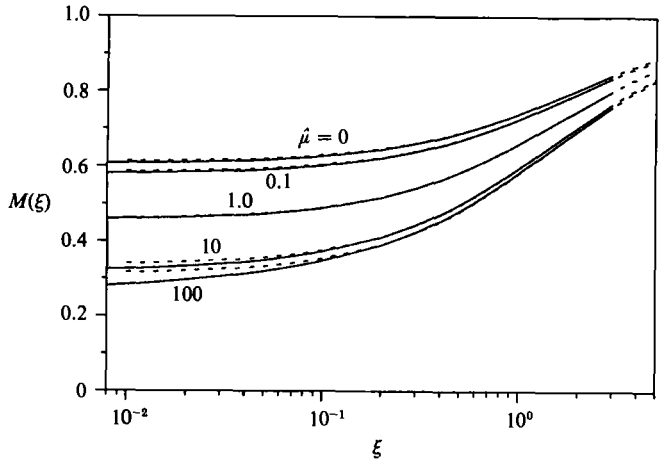

FIGURE 4. The relative mobility function M for transverse motion of two spherical drops as a function of the dimensionless distance between drop surfaces for $\lambda = 0.5$, with different $\hat{\mu}$. The solid lines are from the exact solution; the dashed lines are from the far-field solution given by (2.10).

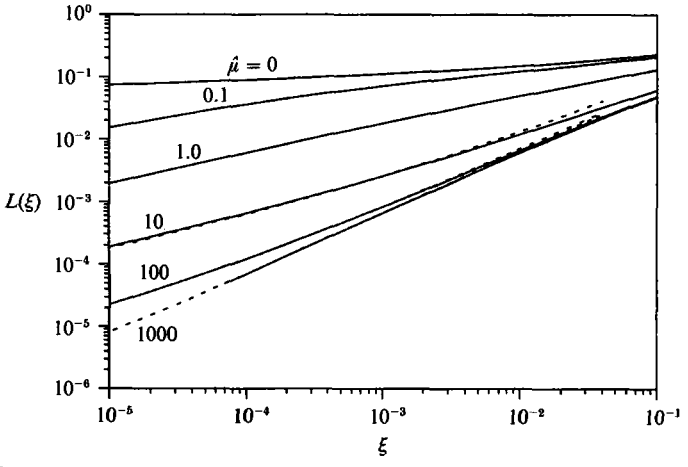

FIGURE 5. The relative mobility function L for axisymmetric motion of two spherical drops as a function of the dimensionless distance between drop surfaces for $\xi \ll 1$ and $\lambda = 0.5$, with different $\hat{\mu}$. The solid lines are from the exact solution; the dashed lines are from the near-field solution given by (2.17) for $\hat{\mu} > 1.0$, or by (2.19) for $\hat{\mu} \leqslant 1.0$.

expansions are accurate to within a few percent for dimensionless separations of $\xi \leqslant O(10^{-3})$. For drops with low viscosity ratios ($\hat{\mu} \leqslant 1$), the near-field solutions given by (2.19) and (2.20) for L and G, respectively, are used instead of (2.17) and (2.18). The results are essentially identical to the exact solution for all $\xi \leqslant O(10^{-1})$.

Of particular interest is the behaviour of the mobility functions for the drops with high viscosity ratios. When the drops are very close together ($\xi \ll 1$), the mobility functions depend strongly on the viscosity ratio. In contrast, the mobility functions for large separations are independent of the viscosity ratio (provided that it is much larger than unity). This is because highly viscous drops behave as rigid spheres with immobile interfaces when they are not close together. It is only when they approach each other closely that their interfaces become mobile and the fluid being squeezed out from between them is able to exert a sufficient tangential stress to drive a flow within the drop phase, thereby influencing the relative mobility functions.

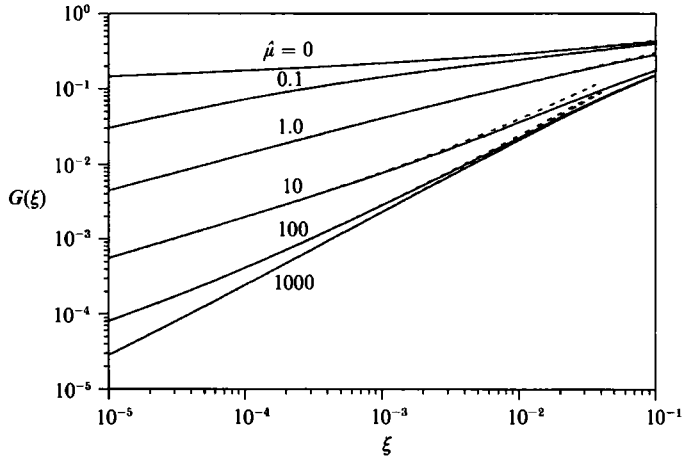

FIGURE 6. The relative mobility function G for the axisymmetric motion of two spherical drops as a function of the dimensionless distance between drop surfaces for $\xi \ll 1$ and $\lambda = 0.5$, with different $\hat{\mu}$. The solid lines are from the exact solution; the dashed lines are from the near-field solution given by (2.18) for $\hat{\mu} > 1.0$, or by (2.20) for $\hat{\mu} \leqslant 1.0$.

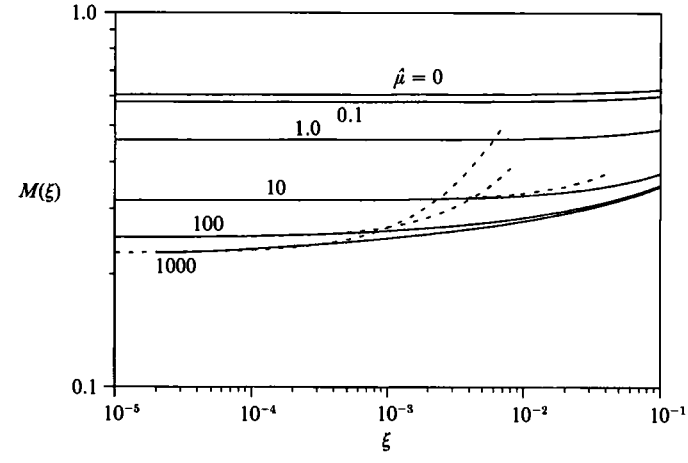

FIGURE 7. The relative mobility function M for the transverse motion of two spherical drops as a function of the dimensionless distance between drop surfaces for $\xi \ll 1$ and $\lambda = 0.5$, with different $\hat{\mu}$. The solid lines are from the exact solution; the dashed lines are from the near-field solution given by (2.21).

3. Expressions for the drop collision rate

We consider here a dispersion with a distribution of drop sizes, and seek to predict the average rate of collisions between drops of size category 1 with those of size category 2 at a given time. The rate at which the drops of radius a_1 collide with the drops of radius a_2 per unit volume is equal to the flux of pairs into the contact surface $r = a_1 + a_2$ and is expressed in terms of the pair-distribution function $p_{12}(\boldsymbol{r})$ and the drop relative velocity $\boldsymbol{V}_{12}$ by

$$J_{12} = -n_1 n_2 \int_{r=a_1+a_2} p_{12}\, \boldsymbol{V}_{12} \cdot \boldsymbol{n}\, \mathrm{d}A, \tag{3.1}$$

where $\boldsymbol{n} = \boldsymbol{r}/r$ is the outward unit normal to the spherical surface represented by

$r = a_1 + a_2$, and n_1 and n_2 are the number of drops at the given time in the size categories characterized by radius a_1 and radius a_2, respectively, per unit volume of the dispersion.

For a dilute dispersion, the pair-distribution function is governed by a quasi-steady mass conservation equation for regions of space outside the contact surface:

$$\nabla \cdot (p_{12} V_{12}) = 0. \tag{3.2}$$

As the colliding drops come into contact, they are assumed to coalesce, and so $p_{12} = 0$ for $r = a_1 + a_2$. Provided that all of the drop–drop encounters originate at wide separations in a homogeneous dispersion, the other boundary condition is $p_{12} \to 1$ as $r \to \infty$.

3.1. *The rate of Brownian collisions*

For drops which are submicron, have densities closely matched with the surrounding fluid, and/or are suspended under microgravity conditions, both Pe and Q_{12} are small compared to unity. In this case, gravity sedimentation is small compared to motion induced by interparticle forces and Brownian diffusion. Carrying out the vector and tensor operations indicated by (2.1), and noting that the Φ_{12} and p_{12} depend on r only owing to the spherical symmetry of Brownian diffusion, then yields:

$$V_{12} = -\frac{D_{12}^{(0)}}{kT} G \left(\frac{\mathrm{d}\Phi_{12}}{\mathrm{d}r} + kT \frac{\mathrm{d} \ln p_{12}}{\mathrm{d}r} \right) \frac{\boldsymbol{r}}{r}. \tag{3.3}$$

It is straightforward to combine this with (3.2) and then integrate twice to obtain the pair-distribution function:

$$p_{12}(r) = \exp(-\Phi_{12}/kT) \frac{\displaystyle\int_{a_1+a_2}^{r} \frac{\exp(\Phi_{12}/kT)}{r^2 G} \mathrm{d}r}{\displaystyle\int_{a_1+a_2}^{\infty} \frac{\exp(\Phi_{12}/kT)}{r^2 G} \mathrm{d}r}. \tag{3.4}$$

Also, the collision rate per unit volume is found by integrating (3.2) only once and then using (3.1) to give

$$J_{12} = \frac{4\pi n_1 n_2 D_{12}^{(0)}}{\displaystyle\int_{a_1+a_2}^{\infty} \frac{\exp(\Phi_{12}/kT)}{r^2 G} \mathrm{d}r}. \tag{3.5}$$

If the drops are assumed to move independently, that is, without any hydrodynamic interactions ($G = 1$) or interparticle forces ($\Phi_{12} = 0$), other than a sticking force on contact, the collision rate is that obtained by Smoluchowski (1917):

$$J_{12}^{(0)} = 4\pi n_1 n_2 D_{12}^{(0)} (a_1 + a_2). \tag{3.6}$$

We define the collision efficiency, $E_{12} \equiv J_{12}/J_{12}^{(0)}$, as the ratio of the predicted collision rate with hydrodynamic and interparticle interactions to that obtained in their absence. Using the dimensionless centre-to-centre distance, $s \equiv 2r/(a_1 + a_2)$, this is then

$$E_{12} = \left(2 \int_2^{\infty} \frac{\exp(\Phi_{12}(s)/kT)}{s^2 G(s)} \mathrm{d}s \right)^{-1}. \tag{3.7}$$

Note that the inverse of the collision efficiency is often called the 'stability ratio' by colloid scientists.

Of considerable interest is the influence of the viscosity ratio on the collision efficiency. For viscous drops, the relative mobility function G for near-contact relative motion is inversely proportional to the square root of the distance between

the drops when the interface mobility is large. It leads to the integration in (3.7) being *finite instead* of being *infinite* as for rigid spheres. Furthermore, since G decreases with increasing viscosity ratio (see figures 3 and 6), (3.7) indicates that the collision efficiency will decrease monotonically as the ratio of the drop-phase viscosity to the suspending-phase viscosity is increased. On the other hand, comparing the effects of the hydrodynamic interactions and the interparticle forces, which are represented by G and Φ_{12}, respectively, on E_{12} through (3.7), it is seen that the hydrodynamic interactions appear in a pre-exponential factor and therefore are subordinate, for moderate values of A/kT, to the interparticle forces, which appear in the argument of the exponential.

3.2. *The rate of gravity-induced collisions*

For supramicron drops having $Pe \gg 1$, Brownian motion is negligible relative to gravity sedimentation. In this case, the relative motion of two drops of different size is deterministic, and the collision rate may then be found using a trajectory analysis. Using (3.2) and the divergence theorem, the integral in (3.1) is taken over the surface which encloses the volume occupied by all trajectories that originate at $r = \infty$ and terminate with the drops coming into contact. The cross-section of this volume at $r = \infty$ is a circle of radius y_c^* due to the symmetry of gravitational motion, and since $p_{12} = 1$ and $V_{12} = V_{12}^{(0)}$ at $r = \infty$, the collision rate is then

$$J_{12} = n_1 n_2 V_{12}^{(0)} \pi y_c^{*2}. \tag{3.8}$$

For rectilinear approach without interactions up to the instant of contact, as in Smoluchowski's model, $y_c^* = a_1 + a_2$, and the collision rate becomes

$$J_{12}^{(0)} = n_1 n_2 V_{12}^{(0)} \pi (a_1 + a_2)^2. \tag{3.9}$$

The collision efficiency is therefore

$$E_{12} \equiv J_{12}/J_{12}^{(0)} = \frac{y_c^{*2}}{(a_1 + a_2)^2}. \tag{3.10}$$

Our problem to determine the collision rate is now reduced to one of determining the critical impact parameter, y_c^*, which is equal to the largest horizontal displacement from the vertical axis of symmetry ($\boldsymbol{g}$ being in the vertical direction, as shown in figure 1) possible for two widely separated drops that eventually will collide. It is determined by solving the trajectory equation to follow this 'limiting' trajectory.

For $Pe \gg 1$, the dimensionless relative velocity $\boldsymbol{u}_{12}$ is given by (2.4) with the last term vanishing:

$$\boldsymbol{u}_{12} = -L(s)\cos\theta\,\boldsymbol{e}_r + M(s)\sin\theta\,\boldsymbol{e}_\theta - \frac{G(s)}{Q_{12}}\frac{\mathrm{d}\phi_{12}}{\mathrm{d}s}\boldsymbol{e}_r. \tag{3.11}$$

The interparticle force term is retained, even if $Q_{12} \gg 1$, because the interparticle forces may become large when the drops are very close together. By decomposing the relative velocity given by (3.11) into the components along and normal to the line of centres (i.e. in the radial and tangential directions) and dividing the radial component by the tangential component, we obtain the trajectory equation:

$$\frac{\mathrm{d}s}{\mathrm{d}\theta} = s\frac{-\left(L(s)\cos\theta + \dfrac{G(s)}{Q_{12}}\dfrac{\mathrm{d}\phi_{12}}{\mathrm{d}s}\right)}{M(s)\sin\theta}. \tag{3.12}$$

As mentioned earlier, the interface mobility of spherical drops allows collision to occur in finite time under the action of a finite force. Considering this situation with

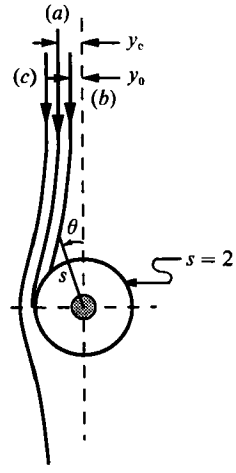

FIGURE 8. Schematic for a binary collision between different-sized drops under the action of gravitational forces only: (*a*) the limiting trajectory; (*b*) a trajectory terminating with contact; (*c*) a trajectory in which the drops move past one another and separate.

the interparticle forces neglected, that is, when the second term in the numerator on the right-hand side of (3.12) is zero, the trajectory equation is reduced to

$$\frac{\mathrm{d}s}{\mathrm{d}\theta} = s\frac{-L(s)\cos\theta}{M(S)\sin\theta}. \tag{3.13}$$

Separating and integrating (3.13) subject to an initial condition $s = s_0$ and $\theta = \theta_0$ at the beginning of the trajectory yields:

$$\sin\theta = \sin\theta_0 \exp\left(\int_s^{s_0} \frac{M}{sL}\mathrm{d}s\right). \tag{3.14}$$

By defining $y_0 = 2y_0^*/(a_1+a_2)$ as the dimensionless initial horizontal distance between the two drops, so that $y_0 = s_0\sin\theta_0$, and then letting $s_0 \to \infty$ as the widely separated initial condition, (3.14) may be rewritten as

$$\frac{y_0}{s\sin\theta} = \exp\left(\int_s^{\infty} \frac{L-M}{sL}\mathrm{d}s\right). \tag{3.15}$$

This equation may be solved for the relative trajectory, $\theta(s)$, which depends on a single parameter, y_0, known as the dimensionless impact parameter.

The dimensionless critical impact parameter, $y_c = 2y_c^*/(a_1+a_2)$, is the value of y_0 that leads to the two drops just grazing each other, as shown in figure 8, and their relative trajectory is then defined as the limiting trajectory. For $y_0 < y_c$, the drops collide; for $y_0 > y_c$, the drops move past one another without colliding. In the absence of interparticle forces, the limiting trajectory is one with the final condition $s = 2$ (contact) when $\theta = \frac{1}{2}\pi$, since by symmetry the point of closest approach occurs at $\theta = \frac{1}{2}\pi$. Using the final condition in (3.15) yields

$$y_c = 2\exp\left(-\int_2^{\infty} \frac{M-L}{sL}\mathrm{d}s\right). \tag{3.16}$$

The collision efficiency defined by (3.10) is then

$$E_{12} = \tfrac{1}{4}y_c^2 = \exp\left(-2\int_2^{\infty} \frac{M-L}{sL}\mathrm{d}s\right). \tag{3.17}$$

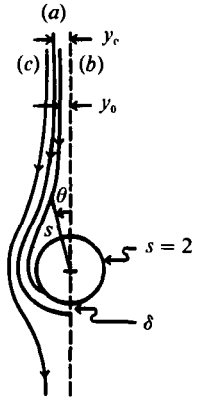

FIGURE 9. Schematic for a binary collision between different-sized drops under the action of gravitational forces and van der Waals attraction: (*a*) the limiting trajectory; (*b*) a trajectory terminating with contact; (*c*) a trajectory in which the drop moves past one another and separate.

With interparticle forces considered, the trajectory equation can no longer be solved analytically for an explicit formula for the dimensionless critical impact parameter, y_c, and hence the collision efficiency. Instead, the determination of the collision efficiency has to be performed by integrating (3.12) numerically along the limiting trajectory from the infinite separation of two drops to the termination point. Since the attractive force pulling the drops together increases with decreasing separation, whereas the gravitational force pulling them apart increases with decreasing $\cos\theta$, the termination point of the limiting trajectory occurs where the larger drop is directly below the smaller drop ($\theta = \pi$) and the van der Waals attraction just balances the gravitational force. This balance occurs when $\xi = \delta$, defined such that $L-(G/Q_{12})\,(\mathrm{d}\phi_{12}/\mathrm{d}s) = 0$. As shown in figure 9, any relative trajectories which are inside this limiting trajectory end with the drops colliding due to the van der Waals attraction, whereas those outside the limiting trajectory end with the drops separating. Note that, in the absence of inertia, the trajectories do not cross.

The dimensionless critical impact parameter may be determined by integrating (3.12) backwards along the limiting trajectory from the termination point $\theta = \pi$ and $\xi = \delta$, to a position $s = s_f$ and $\theta = \theta_f$, beyond which the van der Waals forces are negligible. This numerical solution may be matched with the solution in the outer region ($s > s_f$). Since van der Waals forces are negligible in this outer region, the solution for the limiting trajectory therefore is given by (3.15) with $y_0 = y_c$. Setting $s = s_f$ and $\theta = \theta_f$ as the matching condition reveals that

$$E_{12} = \tfrac{1}{4}y_c^2 = \frac{1}{4}\left[s_f \sin\theta_f \exp\left(\int_{s_f}^{\infty} \frac{L-M}{sL}\,\mathrm{d}s\right)\right]^2. \tag{3.18}$$

4. Results and discussion

4.1. *Brownian collisions without interparticle fores*

With interparticle forces neglected ($\Phi_{12} = 0$), equation (3.7) for the collision efficiency of Brownian drops reduces to

$$E_{12} = \left(2\int_2^{\infty} \frac{1}{s^2 G(s)}\,\mathrm{d}s\right)^{-1}. \tag{4.1}$$

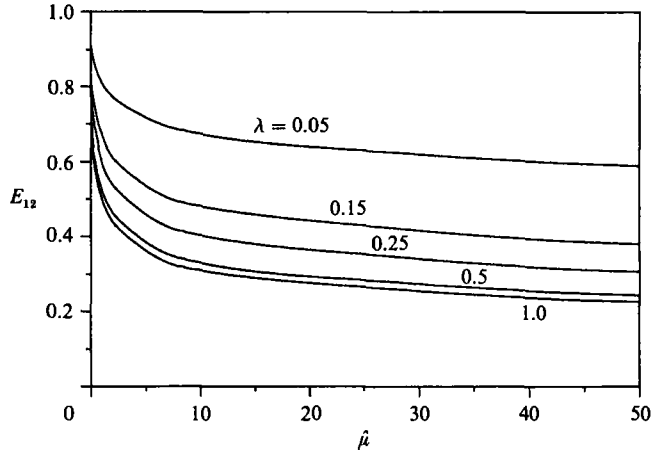

FIGURE 10. The collision efficiency for Brownian drops as a function of the viscosity ratio for various size ratios without interparticle forces.

The calculation of E_{12} can be performed by numerical integration. However, the integration given by (4.1) has a singularity for $\xi \equiv s-2 \to 0$. This singularity was subtracted off and then evaluated analytically using (2.13) and (2.18) for finite $\hat{\mu}$. For bubbles ($\hat{\mu} \to 0$), the singularity as $\xi \to 0$ is sufficiently weak that this was not required. The tail integral for $s \to \infty$ was also evaluated analytically using (2.9) for $s > 7.0$. The remainder of the integral was performed numerically using Simpson's rule together with the series solution of Haber *et al.* (1973) in order to calculate the mobility function G. The number of integration intervals was set to achieve convergence within 0.1%, and a successively decreasing interval was used to account for the more rapid variation of the integrand with decreasing drop separation.

The results for E_{12} as a function of $\hat{\mu}$ are shown in figure 10 for $\lambda = 0.05, 0.15, 0.25, 0.5$, and 1.0. The results are unchanged when λ is replaced by λ^{-1}. As expected, E_{12} decreases as $\hat{\mu}$ increases because this corresponds to decreasing the interface mobility and internal drop flow, which leads to a higher hydrodynamic resistance to close approach. In the limit as $\hat{\mu} \to \infty$, corresponding to that of rigid spheres, $E_{12} \to 0$, although this limit is approached only slowly. Figure 11 shows the results for E_{12} as a function of λ for $\hat{\mu} = 0$, 0.1, 1.0, 10, 100, and 1000. As λ decreases from unity, E_{12} increases and it tends to unity when λ tends to zero. One reason for this is that when λ decreases, the influence of the smaller drop on the Brownian diffusion of the larger one is decreased. Of more importance is that the contribution of the smaller drop to the relative Brownian diffusivity increases as λ decreases. As $\lambda \to 0$, the hydrodynamic interactions become important only within an increasingly small boundary layer around the larger drop, and so $E_{12} \to 1.0$ as $\lambda \to 0$.

4.2. *Brownian collisions with van der Waals forces*

The collision efficiency of drops subject to Brownian diffusion and accounting both for hydrodynamic interactions, which are described by the relative mobility function G, and for unretarded attractive van der Waals forces, whose potentials are expressed by (2.5), was determined by performing the integration in (3.7). An analytical integration for small ξ is not required because the presence of the van der Waals attraction, which has the opposite effect to that of the hydrodynamic interactions, removes the singularity in the integrand. Also, the tail portion of the

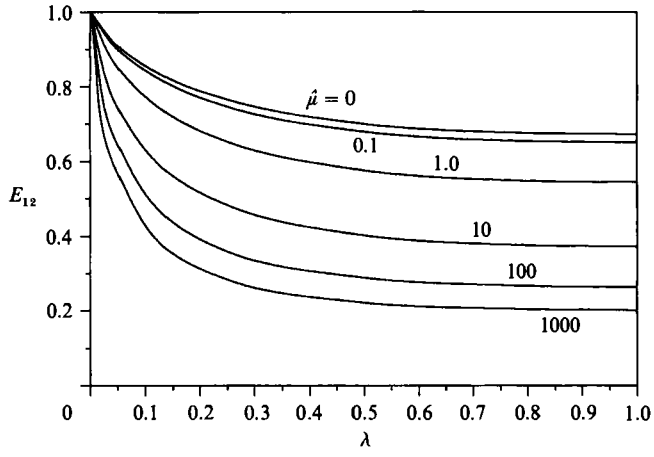

FIGURE 11. The collision efficiency for Brownian drops as a function of the size ratio for various viscosity ratios without interparticle forces.

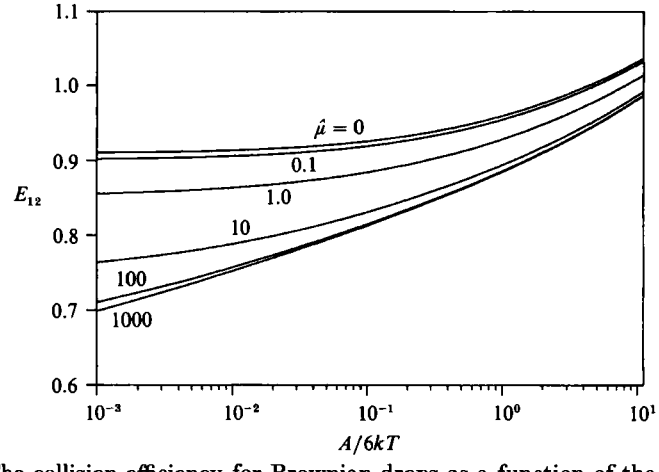

FIGURE 12. The collision efficiency for Brownian drops as a function of the Hamaker group for $\lambda = 0.05$ and various viscosity ratios with unretarded van der Waals attraction.

integral for large separations is unchanged because the van der Waals potential decays as $O(s^{-6})$ for large separations and therefore is of smaller order than the far-field hydrodynamic interactions. In addition to λ and $\hat{\mu}$, the collision efficiency depends upon $A/6kT$. This dimensionless parameter is called the Hamaker group, and it provides a measure of the strength of the van der Waals forces relative to the Brownian motion. It is typically of order unity, or less.

The effects of van der Waals attractions on the collision efficiency of Brownian drops are shown as a function of $A/6kT$ in figures 12–14 for different viscosity ratios, with $\lambda = 0.05$, 0.5, and 1.0, respectively. As expected, the attractive force increases the collision rate. In fact, the collision efficiency becomes larger than unity for $A/6kT \gg 1$, but attractive forces of this magnitude are not usually encountered in practice. Moreover, the van der Waals attraction plays an increasingly important role as $\hat{\mu}$ increases. In particular, the collision efficiency for $\hat{\mu} \gg 1$ is independent of $\hat{\mu}$ at large values of $A/6kT$, but not for small values of $A/6kT$. This is because van der Waals forces are too weak when $A/6kT \ll 1$ to become important until after the

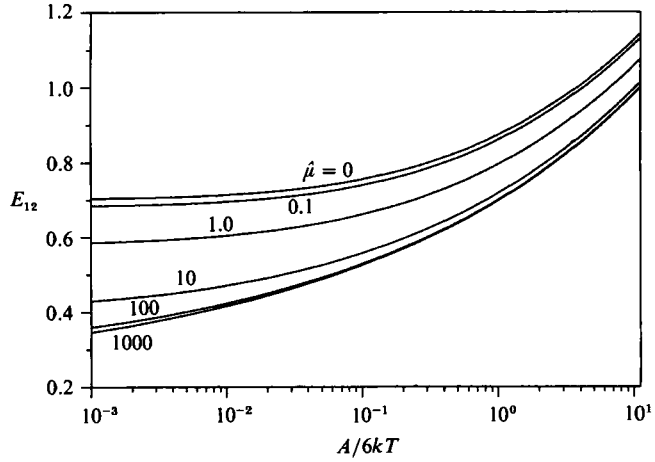

FIGURE 13. The collision efficiency for Brownian drops as a function of the Hamaker group for $\lambda = 0.5$ and various viscosity ratios with unretarded van der Waals attraction.

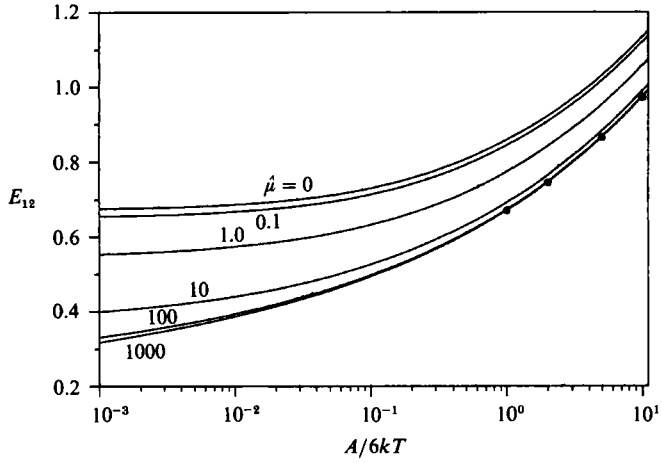

FIGURE 14. The collision efficiency for Brownian drops as a function of the Hamaker group for $\lambda = 1.0$ and various viscosity ratios with unretarded van der Waals attraction. The solid circles are the calculations by Spielman (1970) for rigid spheres.

viscous drops have become sufficiently close that the squeeze flow in the gap between them causes their interfaces to become mobile so that the internal flow and viscosity effect the collision process. In contrast, if both $\hat{\mu}$ and $A/6kT$ are large, then the drops are pulled into contact rapidly by the attractive forces before they approach within this range and so the interface mobility and internal flow do not affect the process – the drops behave as rigid spheres. In this limit, our results agree to within 0.2% with the earlier calculations of Spielman (1970), which are shown as filled circles in figure 14 for $\lambda = 1$ and $\hat{\mu} = \infty$.

Electromagnetic retardation may be included in the analysis simply by using (2.6) in place of (2.5) to assess the significance of the retardation. Numerical results of Zhang (1992) for E_{12} with retarded van der Waals attraction show no qualitative change in the effects of van der Waals attractions on the collision efficiency. Retardation has little effect for small A/kT, because then the van der Waals forces

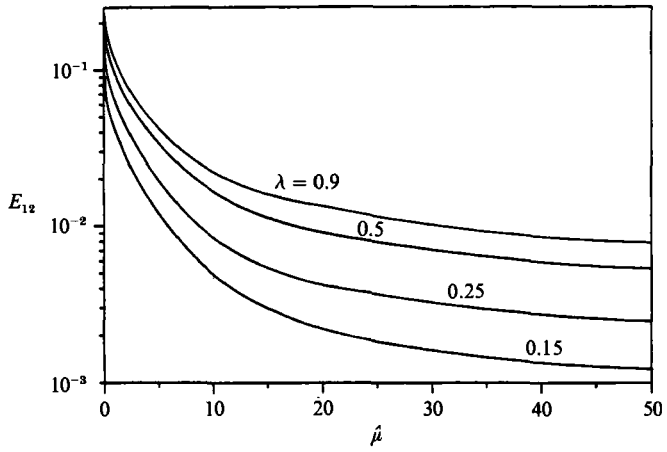

FIGURE 15. The collision efficiency for gravity sedimentation of drops as a function of the viscosity ratio for various size ratios without interparticle forces.

only become significant when the spheres are very close together. For $\nu = 0.5$ and $A/6kT = 0.01$, the reduction in E_{12} due to retardation is less than 10%, whereas it is as much as 25% for $A/6kT = 1.0$.

4.3. *Gravity-induced collisions without interparticle forces*

Neglecting the effects of the interparticle forces, the collision efficiency of sedimenting drops is given by (3.17) and involves an integral of the relative mobility functions. This integral also has a singularity near $s = 2$ which was subtracted off and integrated analytically using (2.17) and (2.21) for finite $\hat{\mu}$. Equations (2.8) and (2.10) were used to evaluate the tail integral analytically for $s > 7.0$. The remainder of the integral was evaluated numerically, with an accuracy of 0.1%, using the series expansions of Haber *et al.* (1973) and Zinchenko (1980) to determine the mobility functions L and M, respectively.

The results for E_{12} as a function of $\hat{\mu}$ are shown in figure 15 for different λ. These results show the expected result that the collision efficiency decreases as $\hat{\mu}$ increases, with $E_{12} \to 0$ only slowly as $\hat{\mu} \to \infty$, as is the case for Brownian collisions. However, the collision efficiencies for gravity collisions are one or two orders-of-magnitude smaller than those for Brownian collisions. Figure 16 shows the results for E_{12} changing with λ, for several different $\hat{\mu}$. The results for the collision efficiencies predicted by Zinchenko (1982) are presented as solid circles for a comparison. There is very good agreement between the present results and Zinchenko's, with the relative difference between them being smaller than 3%. In contrast to the case of Brownian collisions, the collision efficiency decreases as λ decreases. This is because a smaller drop tends to follow the streamlines of the flow around a larger one, and collision does not occur unless the smaller drop is originally on a streamline which is very close to the vertical axis of symmetry. This is also one reason for the collision efficiencies of gravity-induced motion being much smaller than those for Brownian motion. Note from figure 16 that the *collision efficiency* approaches a finite value as the drops become equi-sized ($\lambda \to 1$). However, the *collision rate* goes to zero in this limit because the relative velocity of the two drops approaches zero. By using (2.2) and (3.9), the collision rate may be non-dimensionalized with a quantity not involving the size ratio: $J_{12}/(n_1 n_2 U_1^{(0)} \pi a_1^2) = E_{12}(1-\lambda^2)(1+\lambda)^2$. This quantity is

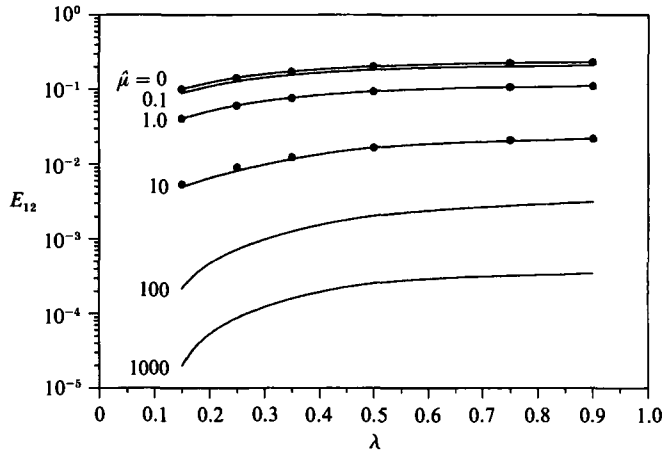

FIGURE 16. The collision efficiency for gravity sedimentation of drops as a function of the size ratio for various viscosity ratios without interparticle forces. The solid circles are the previous results of Zinchenko (1982).

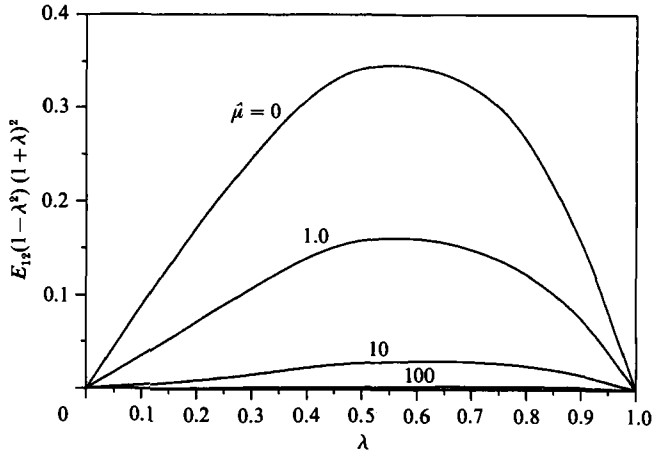

FIGURE 17. The dimensionless collision rate, $J_{12}/(n_1 n_2 U_1^{(0)} \pi a_1^2) = E_{12}(1-\lambda^2)(1+\lambda)^2$, for gravity sedimentation of drops as a function of the size ratio for various viscosity ratios without interparticle forces.

shown in figure 17. The collision rate is small for small size ratios because of the reduced collision cross-section and collision efficiency (as discussed previously), achieves a maximum at moderate size ratio, and then decreases as the size ratio approaches unity because of the reduced relative velocity.

4.4. *Gravity-induced collisions with van der Waals attraction*

In order to avoid numerical difficulties, (3.12) for the trajectories with gravity and van der Waals forces was integrated from θ_f to $\theta = \pi$, forward rather than backward, using the exact solutions for L, G and M and the fourth-order Runge–Kutta method. By systematically varying the matching angle, θ_f, a limiting value, from which the drop flows along the limiting trajectory and finally arrives at the termination point, was determined. The matching separation, s_f, was set to be 9.0 in order to ensure that

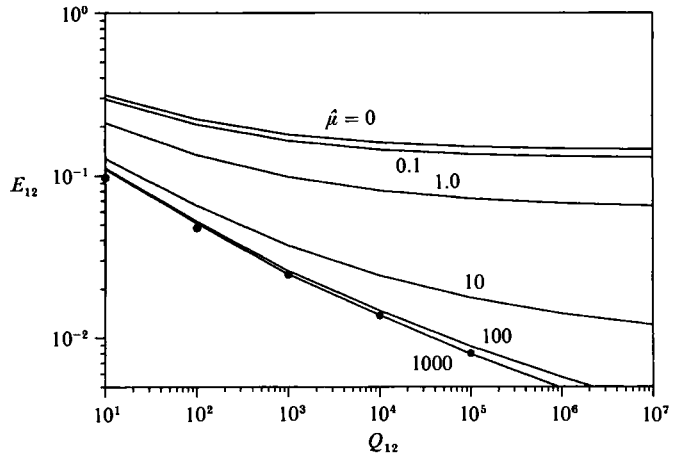

FIGURE 18. The collision efficiency for gravity sedimentation of drops as a function of the interparticle force parameter for $\lambda = 0.25$ and various viscosity ratios with unretarded van der Waals attractions. The solid circles are the rigid-sphere results of Davis (1984).

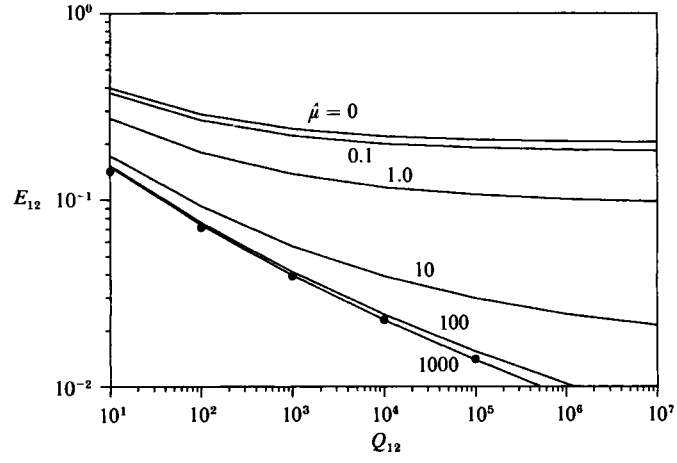

FIGURE 19. The collision efficiency for gravity sedimentation of drops as a function of the interparticle force parameter for $\lambda = 0.5$ and various viscosity ratios with unretarded van der Waals attractions. The solid circles are the rigid-sphere results of Davis (1984).

the van der Waals forces were negligible and that the far-field asymptotic solutions for L, G, and M applied beyond this point. Once the limiting condition, θ_f, was found, the collision efficiency was determined from (3.18).

Typical results for the collision efficiency as a function of the parameter Q_{12} are shown in figures 18–20 for $\lambda = 0.25$, 0.5, and 0.9, respectively, with various $\hat{\mu}$, where the corresponding results of Davis (1984) for rigid spheres are shown as solid circles. In the limit of $\hat{\mu} \to \infty$, there is excellent agreement between our new results and those of Davis (1984). As expected, the collision efficiency increases with increasing values of the Hamaker constant. The collision rate is more sensitive to the van der Waals attraction for drops with high viscosities relative to the surrounding fluid than for drops with moderate or low viscosities. This is because drops with high viscosities offer considerable resistance to near-contact relative motion, which must be

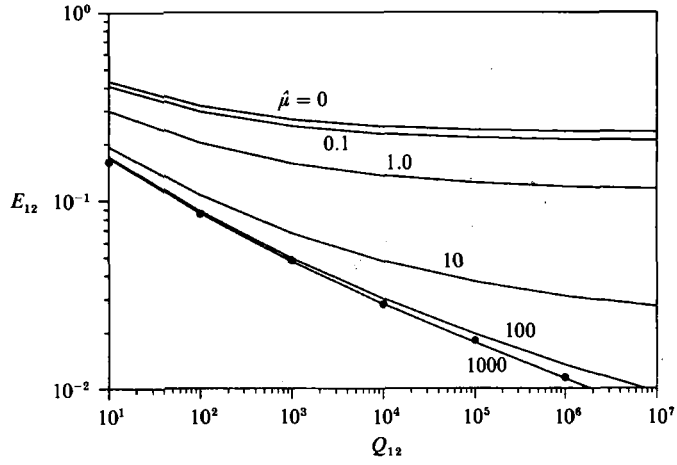

FIGURE 20. The collision efficiency for gravity sedimentation of drops as a function of the interparticle force parameter for $\lambda = 0.90$ and various viscosity ratios with unretarded van der Waals attractions. The solid circles are the rigid-sphere results of Davis (1984).

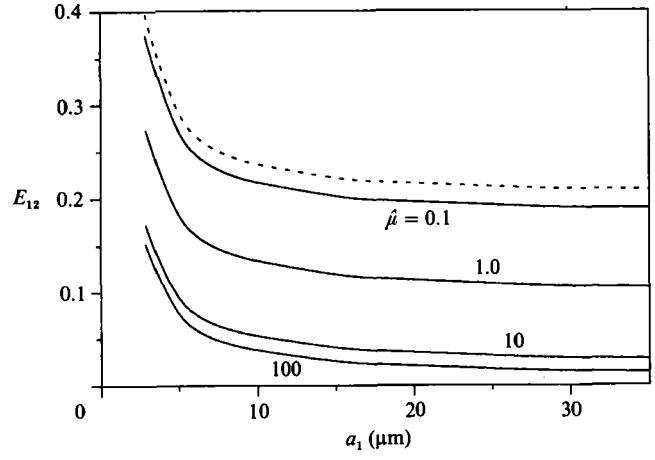

FIGURE 21. The collision efficiency for gravity-induced sedimentation of drops as a function of the radius of the larger drop for a typical hydrosol having $\Delta\rho = 0.1$ cm^3, $kT = 4 \times 10^{-14}$ erg, and $A = 5 \times 10^{-14}$ erg, for $\lambda = 0.5$ and various viscosity ratios. The dashed line is the result for air bubbles in water.

overcome by van der Waals attraction for collisions to occur, whereas the internal flow for drops with low viscosities allows them to collide with relatively small resistance and without the aid of an attractive force.

4.5. *Collision efficiencies for typical hydrosols*

In order for us to gain a better understanding of drop collision processes, the collision efficiency as a function of the radius of the larger drop, a_1, has been calculated for typical hydrosol dispersions, for which values of relative properties are chosen to be $g = 981$ cm/s^2, $\Delta\rho \equiv |\rho' - \rho| = 0.1$ g/cm^3, $A = 5 \times 10^{-14}$ erg, and $kT = 4 \times 10^{-14}$ erg. For this system, $Pe = 0.514\lambda(1-\lambda^2)a_1^4$, where a_1 is in microns, and $Q_{12} = 0.8Pe$. Thus, $Pe > 10$ for $a_1 > 3$ μm and moderate λ, and figure 21 shows the gravitational collision efficiency for $\lambda = 0.5$ as a function of a_1 and several viscosity ratios for this case. The

collision efficiencies are on the order of 0.1 for moderate sizes and viscosity ratios. They decrease as a_1 increases because the strength of the van der Waals force relative to the gravity force, as measured by Q_{12}^{-1}, decreases. The dashed line in figure 21 represents the specific case of air bubbles in water, for which $A = 5 \times 10^{-13}$ erg, $\Delta\rho = 1.0\,\mathrm{g/cm^3}$, and $\hat{\mu} = 0.02$.

When $Pe < 0.1$, or $a_1 < 1\ \mu$m for the system described above, Brownian collisions are expected to dominate over gravitational collisions. Since the Brownian collision efficiency depends only on λ, $\hat{\mu}$, and $A/6kT$, it does not vary with drop size (provided that the condition $Pe \ll 1$ is met) and may be determined for any physical system from figures 10–14 given earlier.

5. Conclusions

Quantitative predictions of the collision rate of two spherical drops undergoing Brownian diffusion or gravitational sedimentation are presented in this work. By solving the diffusion equation for relative Brownian motion of two drops, and using a trajectory analysis to follow the relative motion of pairs of drops in gravitational sedimentation, we have developed theoretical models to determine the collision efficiencies, both with and without interparticle forces applied between the drops. From these models, it is concluded that finite collision rates between non-deforming fluid drops are possible for Brownian diffusion or gravitational sedimentation in the absence of attractive forces, in stark contrast to the prediction that lubrication forces prevent rigid spheres from contacting each other unless an attractive force that becomes infinite as the separation approaches zero is applied. Collision rates are shown to increase as the viscosity of the drop-phase decreases. This is because the squeeze flow of fluid out of the gap separating two approaching drops drives a flow inside the drops; the viscous resistance of this internal flow exerted on the external squeeze flow decreases as the viscosity of the internal phase relative to that of the external phase decreases. In general, hydrodynamic interactions reduce the collision rates more for gravitational collisions than for Brownian collisions.

We conclude with some comments regarding the limitations of the present study. One underlying restriction is that the flow in and around the drops is sufficiently slow that inertia is small relative to viscous forces. This requires that the Reynolds number, $Re \equiv \rho U a/\mu$, be small compared to unity for all phases, where a is the larger drop radius and U is its sedimentation velocity. For typical conditions of $\mu = 0.01\,\mathrm{g/cm\,s}$, $\rho = 1\,\mathrm{g/cm^3}$, $\Delta\rho = 0.1\,\mathrm{g/cm^3}$, and $g = 10^3\,\mathrm{cm/s^2}$, this requires that $a \leqslant 50\ \mu$m.

Another restriction is that the drops remain spherical. Yiantsios & Davis (1991) have shown that this requires that the modified capillary number, $Ca \equiv \mu U a/\sigma h_0$, be small compared to unity, where σ is the interfacial tension and h_0 is the distance separating the drops at the point of nearest contact. For the typical value of $\sigma = 10\,\mathrm{dyne/cm}$, this condition is also met for $a \leqslant 50\ \mu$m, provided that $h_0 > 0.002a$. However, when the drops become closer than this, the pressure which builds up to drive the external fluid out of the gap between them will also cause the interfaces to deform by an amount that is comparable to the minimum separation distance. As described in detail by Yiantsios & Davis (1991), this deformation will actually prevent the surfaces from coming into contact, unless an attractive force is present. Fortunately, the separation distance at which van der Waals attraction becomes comparable to the gravity force, $h_0 = (A/6\pi\mu U)^{\frac{1}{2}}$, is larger than this for $A = 5 \times 10^{-14}$ erg, provided that $a \leqslant 100\ \mu$m. Thus, we expect our analysis neglecting both inertia

and deformation to be reasonable for drops smaller than about 100 μm in diameter for many typical systems.

As mentioned previously, our analysis does not include the presence of interparticle repulsive forces. Since such forces between drops are usually associated with surfactants on drop interfaces which greatly reduce their mobility, it is anticipated that previous analyses for rigid spheres will provide a reasonable approximation for the behaviour of drops with repulsive forces. Finally, our analysis considers Brownian motion and gravity sedimentation independently. Both will be important for drops in the micron size range having $Pe = O(1)$. For these, the complete convection-diffusion equation (2.1), would need to be solved, with some progress possible using perturbation methods.

This paper is based upon work supported by NASA grant NAG3–993 and by NSF grant CTS–8914236. We also thank Dr N. Hill for helpful discussions and Dr A. Zinchenko for providing details of his calculations.

REFERENCES

BATCHELOR, G. K. 1982 Sedimentation in a dilute polydisperse system of interacting spheres. *J. Fluid Mech.* **119**, 379–408.

DAVIS, R. H. 1984 The rate of coagulation of a dilute polydisperse system of sedimenting spheres. *J. Fluid Mech.* **145**, 179–199.

DAVIS, R. H., SCHONBERG, J. A. & RALLISON, J. M. 1989 The lubrication force between two iscous drops. *Phys. Fluids* A1, 77–81.

DERJAGUIN, B. & LANDAU, L. 1941 Theory of the stability of strongly charged lyophobic sols and of the adhesion of strongly charged particles in solution of electrolytes. *Acta. Physicochim.* **14**, 633.

FUENTES, Y. O., KIM, S. & JEFFREY, D. J. 1988 Mobility functions for two unequal viscous drops in Stokes flow. Part 1. Axisymmetric motions. *Phys. Fluids* **31**, 2445–2455.

FUENTES, Y. O., KIM, S. & JEFFREY, D. J. 1989 Mobility functions for two unequal viscous drops in Stokes flow. Part 2. Nonaxisymmetric motions. *Phys. Fluids* A1, 61–76.

HABER, S., HETSRONI, G. & SOLAN, A. 1973 On the low Reynolds number motion of two droplets. *Intl J. Multiphase Flow* **1**, 57–71.

HAMAKER, H. C. 1937 The London-van der Waals attraction between spherical particles. *Physica* **4**, 1058.

HETSRONI, G. & HABER, S. 1978 Low Reynolds number motion of two drops submerged in an unbounded arbitrary velocity field. *Intl J. Multiphase Flow* **4**, 1–17.

HO, N. F. H. & HIGUCHI, W. I. 1968 Preferential aggregation and coalescence in heterodispersed system. *J. Pharm. Sci.* **57**, 436–442.

KIM, S & ZUKOSKI, C. F. 1990 A model of growth by hetero-coagulation in seeded colloidal dispersions. *J. Colloid Interface Sci.* **139**, 198–212.

LAMB, S. H. 1945 *Hydrodynamics*, p. 600. Dover.

MELIK, D H. 1984 Flocculation in quiescent media. Ph.D. thesis, University of Michigan.

MELIK, D. H. & FOGLER, H. S. 1984 Gravity-induced flocculation. *J. Colloid Interface Sci.* **101**, 72–83.

REED, L. D. & MORRISON, F. A. 1974 The slow motion of two touching fluid spheres along their line of centers. *Intl J. Multiphase Flow* **1**, 573–583.

ROGERS, J. R. & DAVIS, R. H. 1990 The influence of van der Waals attractions on cloud droplet growth by coalescence. *J. Atmos. Sci.* **47**, 1057–1080.

RUSHTON, E. & DAVIES, G. A. 1973 The slow unsteady settling of two fluid spheres along their line of centers. *Appl. Sci. Res.* **28**, 37–61.

SCHENKEL, J. H. & KITCHNER, J. A. 1960 A test of the Derjaguin–Verwey–Overbeek theory with a colloidal suspension. *Trans. Faraday Soc.* **56**, 161.

SMOLUCHOWSKI, M. VON 1917 Versuch einer mathematishen Theorie dar koagulationskinetik kollider Lösungen. *Z. Phys. Chem.* **92**, 129–168.

SPIELMAN, L. A. 1970 Viscous interactions in Brownian coagulation. *J. Colloid Interface Sci.* **33**, 562–571.

VALIOULIS, I. A. & LIST, E. J. 1984 Collision efficiencies of diffusing spherical particles: hydrodynamic, van der Waals and electrostatic forces. *Adv. Colloid Interface Sci.* **20**, 1–20.

VERWEY, E. J. W. & OVERBEEK, J. TH. G. 1948 *Theory of the Stability of Lyophobic Colloids.* Elsevier.

WEN, C.-S. & BATCHELOR, G. K. 1985 The rate of coagulation in a dilute suspension of small particles. *Scientia Sinica* A **28**, 172–184.

YIANTSIOS, S. G. & DAVIS, R. H. 1991 Close approach and deformation of two viscous drops due to gravity and van der Waals forces. *J. Colloid Interface Sci.* (in press).

ZHANG, X. 1992 The collision rate of a dilute polydisperse system of spherical drops. Ph.D. thesis, University of Colorado.

ZINCHENKO, A. Z. 1978 Calculation of hydrodynamic interactions between drops at low Reynolds number. *Prikl. Mat. Mech.* **42**, 955–959.

ZINCHENKO, A. Z. 1980 The slow asymmetric motion of two drops in a viscous medium. *Prikl. Mat. Mech.* **44**, 30–37.

ZINCHENKO, A. Z. 1982 Calculations of the effectiveness of gravitational coagulation of drops with allowance for internal circulation. *Prikl. Mat. Mech.* **46**, 58–65.